Hue University Journal of Science: Natural Science
Vol. 134, No. 1D, 5–22, 2025

pISSN 1859-1388
eISSN 2615-9678

An *in silico* study on the anti-diabetic potential of some compounds from the genus *Cordyceps*

Nguyen Dai Chau[1], Nguyen Cong Kinh[2], Nguyen Thi Thanh Hai[1], Phan Tu Quy[3], Nguyen Vinh Phu[4], Thanh Q. Bui[1], Nguyen Chi Bao[5], Ton That Huu Dat[6], Nguyen Thi Ai Nhung[1]*

[1] Department of Chemistry, University of Sciences, Hue University, Hue 49000, Vietnam
[2] Department of Pharmacy, Duy Tan University, Da nang 50000, Vietnam
[3] Department of Natural Sciences & Technology, Tay Nguyen University, Buon Ma Thuot 630000, Vietnam
[4] Faculty of Basic Sciences, University of Medicine and Pharmacy, Hue University, Hue 49000, Vietnam
[5] Hue University, Hue 49000, Vietnam
[6] Mientrung Institute for Scientific Research, Vietnam National Museum of Nature, Vietnam Academy of Science and Technology (VAST), Hue 49000, Vietnam

* Correspondence to Nguyen Thi Ai Nhung <ntanhung@hueuni.edu.vn>

(*Received: 16 October 2025; Revised: 14 November 2025; Accepted: 12 December 2025*)

Abstract. This study was designed to evaluate the inhibitory potential of nine representative compounds, belonging to the nucleoside, flavonoid, and steroid classes from *Cordyceps* species, against two protein targets: α-amylase (PDB ID: 4W93) and α-glucosidase (PDB ID: 3W37) by means of an *in-silico* approach. Molecular docking simulations identified sites 1 and 2 as the optimal sites for ligand interaction with the two respective proteins. The docking results were validated, with RMSD values of less than 2.0 Å for all complexes. Compound C3 was identified as the most potent inhibitor for protein 4W93, while C2 was the most effective against protein 3W37. According to Lipinski's rule of five, all compounds exhibited favourable "drug-likeness" characteristics, and the pharmacokinetic and toxicological properties of these compounds were further evaluated via ADMET parameter predictions. The complexes, **C3-4W93** and **C2-3W37,** were selected for molecular dynamics simulations. The two complexes are structurally stable throughout the simulation, and the C3 ligand forms the most favourable and persistent interactions with the 4W93 protein.

Keywords: *Cordyceps, in silico, protein 4W93, protein 3W37*

1 Introduction

Diabetes is increasing rapidly worldwide and has become a major health concern. In 2021, 536,6 million people were affected by this disease in the world, and this figure is expected to reach 783.2 million by 2045 [1]. In Vietnam, the prevalence is also rising, with an estimate of 5 million cases in 2021 [2]. Diabetes is a complex metabolic disorder that causes numerous serious complications, such as cardiovascular disease, blindness, and kidney failure. It is classified into two main types: type 1 and type 2 [3], with type 2 accounting for the majority [3, 4]. Modern medical treatment focuses on drug groups that stimulate insulin secretion and inhibit [5]. Therefore, the search for new drugs from natural compounds to replace current commercial drugs is a top priority for scientists, especially the screening of compounds from medical plants with inhibitory ability against α-amylase and α-glucosidase.

The *Cordyceps cicadae* is one of the valuable medicinal fungi, containing various bioactive compounds, which have been shown to exhibit antioxidant, anti-inflammatory, immune-enhancing, and especially blood glucose-regulating effects [6, 7]. Although the medicinal potential of the *Cordyceps* species is considerable,

studies on their chemical composition and biological activities, particularly in Vietnam, remain relatively limited. The application of modern research methods, such as *in-silico* (computer simulation), enables the rapid and efficient screening of the interaction potential of numerous compounds with molecular biological targets, thereby providing direction for experimental studies and reducing both time and cost.

In this study, our group carried out research and selection of representative compounds from the *Cordyceps* genus according to published studies. Subsequently, the inhibitory potential against two enzymes, α-amylase and α-glucosidase, was investigated in an *in-silico* framework using molecular docking simulation. These compounds were screened to obtain drug-likeness following Lipinski's Rule of Five, and their pharmacokinetic and toxicological properties were predicted using the ADMET model.

2 Methods

2.1 Molecular docking simulations

Molecular docking was used to predict docking energies and interactions between the compounds (ligands) and the enzymes/proteins. The entire process was performed with MOE 2022.10, ChemBioOffice 2018, and SYBYL-X 1.1 software packages.

Step 1. Preparation of protein – ligand

+ Protein: The three-dimensional structure of the protein was collected from the Protein Data Bank (PDB). The protein structure was prepared by removing water molecules and unnecessary polymer chains. The binding site was defined on the basis of the position of the co-crystallised ligand.

+ Ligand: The 3D structures of the compounds studied were constructed by using ChemBioOffice 2018 and subsequently energy-minimised with SYBYL-X 1.1 to obtain the optimised structures.

Step 2. Molecular docking and protocol validation

+ Molecular docking: The MOE 2022.10 software was utilised for molecular docking with the following settings: automatic detection of protein cavities compatible with ligand volume; maximum number of results per iteration was set to 1000; and maximum number of results for each ligand fragment was set to 200. The best conformations were selected on the basis of the lowest molecular docking score energy (DS, $kcal.mol^{-1}$).

+ Validation: A molecular re-docking procedure was carried out to ensure the reliability of the selected docking parameters, which was considered acceptable when the root-mean-square deviation (RMSD) between the re-docked conformation and the original crystal conformation was less than 2.0 Å [8].

Step 3. Analysis of results

In order to evaluate the protein inhibitory activity of these compounds, we assessed the docking score and ligand-protein interactions. Noncovalent interactions between the ligand and amino acids in the binding site were analysed and visualised in both 2D and 3D formats. The key interaction types considered included hydrogen bonding, π-π interactions, ionic interactions, cation-π interactions, and hydrophobic (van der Waals) interactions. This analysis helped to clarify the binding mechanism at the molecular level.

Physicochemical analysis

The drug-likeness properties of the phytochemicals were calculated with online bioinformatics tools. Specifically, molecular weight (MW) and partition coefficients (log*P* and log*S*) were determined through the ADMETLab 3.0 server (https://admetlab3.scbdd.com), while polarity-related

pISSN 1859-1388
eISSN 2615-9678

parameters were calculated by using ChemDoodle Web Components (https://web.chemdoodle.com). The references were from Lipinski's rule of five [9], which provides the theoretical criteria for a well membrane-permeable candidate, i.e., molecular mass < 500 Da; hydrogen-bond donors, all criteria for a well membrane ≤10; log*P* < +5 [10, 11].

2.2 ADMET prediction

The pharmacokinetic and toxicological properties were predicted and analysed by using the regression model SwissADME, which was developed and maintained by the Swiss Institute of Bioinformatics, and were theoretically evaluated via the framework proposed by Pires et al. [12] (http://biosig.unimelb.edu.au/pkcsm/theory). The ADMET parameters of the studied compounds, namely absorption, distribution, metabolism, excretion, and toxicity, were predicted.

2.3 Molecular dynamics simulation

The Molecular dynamics (MD) simulation was carried out by using GROMACS 2023 through the following steps:

Step 1. System setup

The protein and ligand were parameterised by using the CHARMM-27 force field (ligand prepared with SwissParam). The system was solvated in water (TIP3P) and neutralised with Na^+/Cl^- ions.

Step 2. Dynamics simulation

Energy minimisation was carried out for 100 ps with a maximum force of 10 kJ/mol, and equilibration was performed at 300 K and 1 bar. The MD simulations were conducted with the Verlet algorithm, whereas the LINCS algorithm was used to restrain hydrogen bonds [13].

Step 3. Analysis of results

After completing the MD simulations, we utilised the data to calculate the RMSD (root-mean-square deviation), the RMSF (root-mean-square fluctuation), the Rg (radius of gyration), and the SASA (solvent-accessible surface area). We employed these parameters to evaluate the stability of the complexes and the effect of ligand binding on the protein. The hydrogen bond formation ratio was also analysed by using VMD software, with criteria of D-A distance < 3.5 Å and D–H···A angle >120°. The binding free energy was computed with the gmx_MMPBSA tool [14] on the basis of GROMACS trajectories using the CHARMM-27 force field combined with the MM/GBSA method under the following conditions: the dielectric constant of 1.0, the temperature of 298 K, and the salt concentration of 0.15 M [15].

3 Results and Discussion

3.1 The input data of the compounds and proteins studied

We focused on the representative compounds from the *Cordyceps* genus according to published studies. The molecular formulas, notation, and chemical structure of the studied compounds are presented in Fig. 1 and Table 1. These compounds were classified into major groups, namely nucleotides (**C1–C3**), flavonoids (**C4–C6**), and steroids (**C7–C9**). For comparison, acarbose (**D**), a commercial antidiabetic drug, was also used as a controlled drug.

Two proteins: 4W93 (https://doi.org/10.2210/pdb4W93/pdb) and 3W37 (https://doi.org/10.2210/pdb3W37/pdb), representing α-amylase and α-glucosidase enzymes, respectively, were studied, and their structure is illustrated in Fig. 2.

Table 1. The data of studied compounds **C1–C9** and controlled drug Acarbose (**D**)

No	Compounds	Notation	Formula	Ref
1	Cordycepin (3′-deoxyadenosine)	**C1**	$C_{10}H_{13}N_5O_3$	
2	Adenosine	**C2**	$C_{10}H_{13}N_5O_4$	[6,16,17]
3	Guanosine	**C3**	$C_{10}H_{13}N_5O_5$	
4	Quercetin	**C4**	$C_{15}H_{10}O_7$	
5	Kaempferol	**C5**	$C_{15}H_{10}O_6$	[18]
6	5,7,3',4',5'-Pentamethoxyflavone	**C6**	$C_{20}H_{20}O_8$	
7	Stigmasterol	**C7**	$C_{29}H_{48}O$	
8	Ergosterol	**C8**	$C_{28}H_{44}O$	[6,19,20]
9	β-Sitosterol	**C9**	$C_{29}H_{50}O$	
10	Acarbose	**D**	$C_{25}H_{43}NO_{18}$	Controlled drug

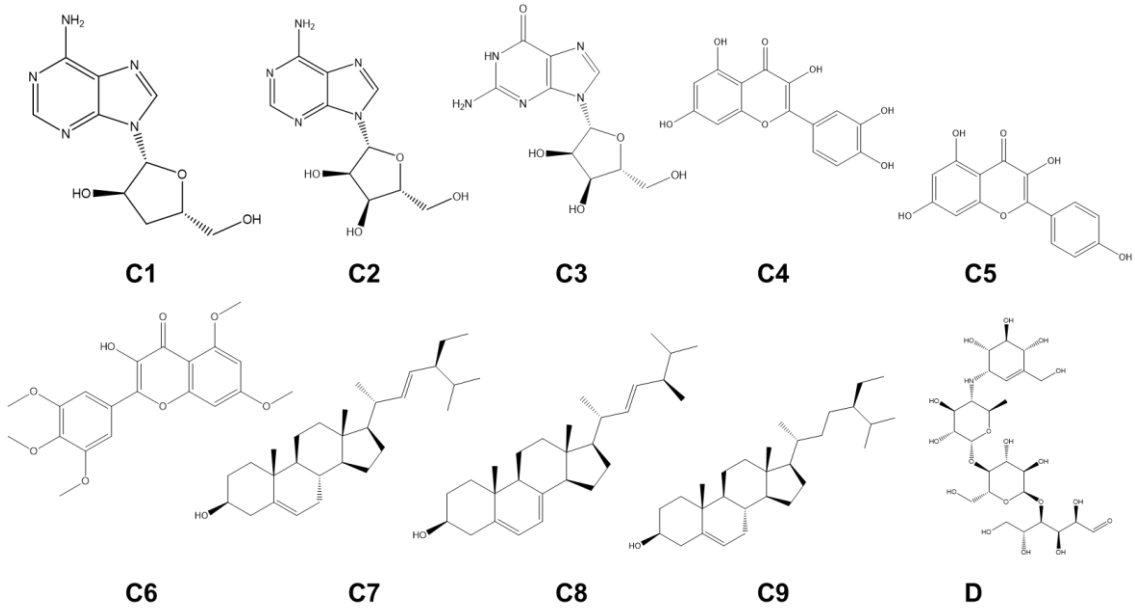

Fig. 1. Chemical structure of studied compounds **C1–C9** and controlled drug Acarbose (**D**)

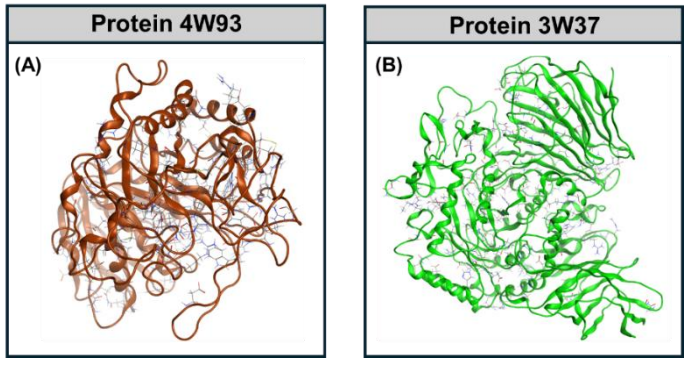

Fig. 2. Crystal structures of (A) α-amylase 4W93 and (B) α-glucosidase 3W37

pISSN 1859-1388
eISSN 2615-9678

3.2 Protein inhibitability

The molecular docking simulation was used to simulate and predict the interaction between the studied compounds and the two proteins. First, the study focuses on examining and screening the binding sites to identify the optimal sites for inhibitory abilities. In addition, the major interactions, such as hydrogen bonds and van der Waals forces, between the studied compounds and the two-target protein were analysed, which help to identify the optimal interaction sites for the protein inhibition.

Fig. 3 presents the quaternary structures of proteins 4W93 and 3W37 with binding pockets for compounds **C1–C9** and acarbose at four sites (1: gray, 2: yellow, 3: green, 4: orange). The optimal binding sites were determined by comparing docking scores and interaction numbers, where lower docking scores and more interactions indicated stronger inhibition. The prescreening results of binding sites for proteins 3W37 and 4W93 are summarised in Table 2. For protein 4W93, the two optimal sites were site 1 (gray) and site 2 (yellow). Compounds **C1** and **C2** exhibited favourable inhibition at site 1, whereas compounds **C3–C9** and acarbose were more compatible with site 2. Similarly, for protein 3W37, site 1 was suitable for compounds **C2–C9** and **D**, while site 2 was optimal for compound **C1**. After prescreening and identifying the optimal sites, we performed molecular docking simulations on proteins 4W93 and 3W37 to evaluate the inhibitory potential of the studied compounds in detail. The docking process provided key parameters such as docking score (DS), RMSD value, van der Waals interactions, and hydrogen bonds, which help to clarify how the protein interacts with the inhibitors and allow a scientific prediction of their potential inhibitory efficiency.

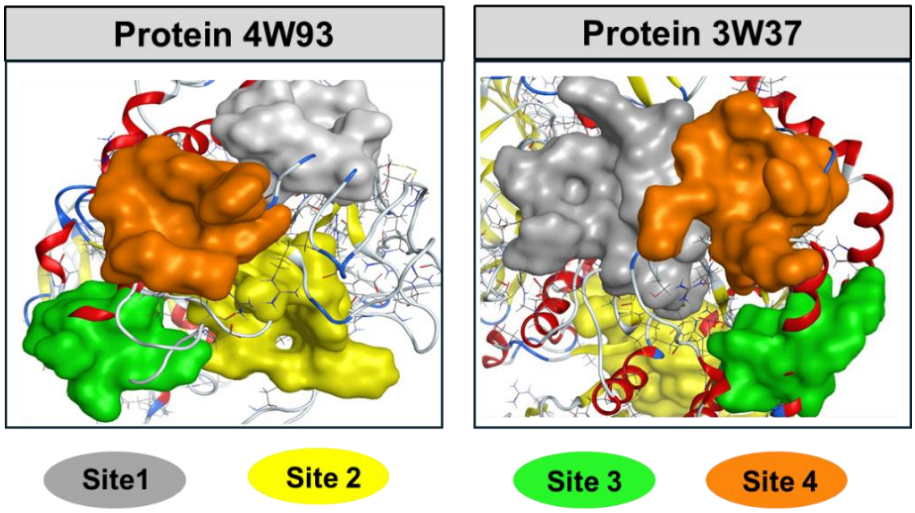

Fig. 3. Quaternary structures of protein 4W93 and 3W37 with the approachable sites by **C1–C9** and the controlled drug Acarbose (**D**): site 1 (yellow), site 2 (gray), site 3 (green), site 4 (orange)

Table 2. Prescreening results on inhibitability of ligands (**C1-C9**) and controlled drug (**D**) towards the sites of proteins 4W93 and 3W37

Ligand-protein		Site 1		Site 2		Site 3		Site 4	
Protein	**Ligand**	**E**	**N**	**E**	**N**	**E**	**N**	**E**	**N**
4W93	**C1**	**-10.7***	**2***	-9.1	1	-9.0	1	-8.3	0
	C2	**-10.9***	**2***	-9.0	1	-8.8	1	-8.5	1

Ligand-protein		Site 1		Site 2		Site 3		Site 4	
Protein	**Ligand**	**E**	**N**	**E**	**N**	**E**	**N**	**E**	**N**
	C3	-10.8	3	**-12.4***	**5***	-10.6	3	-9.7	2
	C4	-9.8	1	**-11.0***	**2***	-9.4	1	-9.0	1
	C5	-8.8	1	**-10.5***	**2***	-7.9	0	-8.5	1
	C6	-7.3	0	**-9.0***	**1***	-7.5	0	-7.0	0
	C7	-9.6	1	**-11.9***	**3***	-9.3	1	-8.5	1
	C8	-7.4	0	**-8.9***	**1***	-7.0	0	-6.8	0
	C9	-9.0	1	**-11.3***	**3***	-9.3	1	-8.9	1
	D	-10.8	2	**-12.0***	**4***	-10.2	2	-9.5	1
3W37	**C1**	-9.2	1	**-11.6***	**3***	-8.8	1	-8.2	1
	C2	**-12.9***	**6***	-10.8	3	-10.5	3	-9.6	2
	C3	**-12.7***	**6***	-10.7	2	-10.9	3	-10.5	3
	C4	**-11.9***	**3***	-9.3	1	-9.1	1	-8.2	0
	C5	**-11.3***	**3***	-10.1	2	-8.9	1	-8.1	1
	C6	**-12.0***	**4***	-10.4	2	-9.9	2	-8.5	1
	C7	**-10.8***	**2***	-9.1	1	-8.2	0	-9.0	1
	C8	**-11.0***	**3***	-10.4	2	-9.6	1	-9.3	1
	C9	**-8.7***	**1***	-8.0	0	-7.6	0	-7.1	0
	D	**-13.0***	**10***	-11.0	4	-10.9	3	-10.7	3

E: DS value (kcal.mol^{-1}); **N**: Number of hydrophilic interactions

Table 3. Molecular docking simulation results for ligands (**C1–C9** and **D**)-4W93 inhibitory complexes

Ligand-protein			Hydrogen bond						Van der Waals interaction
Name	**DS**	**RMSD**	**L**	**P**		**T**	**D**	**E**	
C1-4W93	-10.7	1.60	O	O	Glu 181	H-donor	2.93	-3.5	Leu 69, Glu 76, Tyr 67, Tyr 182, His 185, Lys 178, Val 129
			5-ring	C	Lys 68	π-H	3.64	-1.9	
C2-4W93	-10.9	1.56	O	O	Glu 181	H-donor	3.14	-1.4	Tyr 67, Leu 69, Tyr 182, His 185, Lys 178, Ala 128, Val 129, Glu 76
			5-ring	C	Lys 68	π-H	3.65	-2.0	
C3-4W93	-12.4	1.65	O	O	Glu 233	H-donor	2.98	-2.9	His 299, Asp 197, Asp 300, Arg 195, Ala 198, His 101, Leu 162, Leu 165, Trp 58.
			O	O	Glu 233	H-donor	3.01	-1.9	
			N	O	Asp 356	H-donor	2.98	-6.4	
			N	5-ring	His 305	H-π	3.41	-1.6	
			6-ring	5-ring	Trp 59	π-π	3.01	-1.7	

pISSN 1859-1388
eISSN 2615-9678

Ligand-protein			Hydrogen bond						Van der Waals interaction
Name	**DS**	**RMSD**	**L**	**P**		**T**	**D**	**E**	
C4-4W93	-11.0	1.10	O	O	Glu 233	H-donor	2.90	-4.3	Asp 300, Asp 197, Tyr 62, His 299, Gln 63, Leu 165, His 305, Asp 356, Trp 58.
			6-ring	6-ring	Trp 59	π-π	3.66	-5.8	
C5-4W93	-10.5	1.11	O	O	Asp 197	H-donor	2.98	-4.1	Asp 300, Glu 233, His 299, Tyr 62, Leu 165, Gln 63, His 305, Asp 356, Trp 58.
			6-ring	6-ring	Trp 59	π-π	3.65	-3.4	
C6-4W93	-9.0	0.52	6-ring	N	His 201	π-H	3.94	-0.5	Lys 200, Ala 198, Ile 235, Glu 233, Tyr 62, His 101, Gln 63, Leu 165, Trp 59, Leu 162, Thr 163
C7-4W93	-11.9	1.67	C	5-ring	Trp 59	H-π	3.56	-0.5	Asp 197, Asp 300, Tyr 62, His 299, Ala 198, Gln 63, His 101, Ile 235, Leu 162, His 201, Trp 58, Leu 165, His 305, Glu 233
			C	5-ring	Trp 59	H-π	3.38	-0.6	
			C	6-ring	Trp 59	H-π	3.14	-0.6	
C8-4W93	-8.9	1.05	C	5-ring	His 305	H-π	3.23	-0.7	Ala 198, Glu 233, Asp 197, His 101, Lys 200, Leu 162, Ile 235, Trp 59, His 201, Tyr 62, Trp 58, Asp 300, Gly 308, Asp 356.
C9-4W93	-11.3	1.34	O	NZ	Lys 200	H-acceptor	3.13	-3.8	Tyr 62, His 101, Asp 356, Ile 235, Trp 58, His 201, Asp 197, His 305, Leu 165, Leu 162, Ala 198, Asp 300, Glu 233.
			C	6-ring	Trp 59	H-π	3.21	-0.8	
			C	5-ring	Trp 59	H-π	3.96	-0.5	
D-4W93	-12.0	1.68	O	O	Asp 197	H-donor	3.36	-0.5	Ala 198, His 101, Trp 58, Ile 235, Asp 300, Leu 165, Gly 104, Leu 162, His 305, Thr 163, Gln 63, Gly 164, Ala 108, Lys 200
			O	O	Glu 233	H-donor	3.02	-1.0	
			O	N	His 201	H-acceptor	2.99	-1.1	
			C	6-ring	Trp 59	H-π	3.19	-0.5	

DS: Docking score energy (kcal.mol^{-1}); **RMSD**: Root-mean-square deviation (Å); **L**: Ligand; **P**: Protein; **T**: Type; **D**: Distance (Å); **E**: Energy (kcal.mol^{-1})

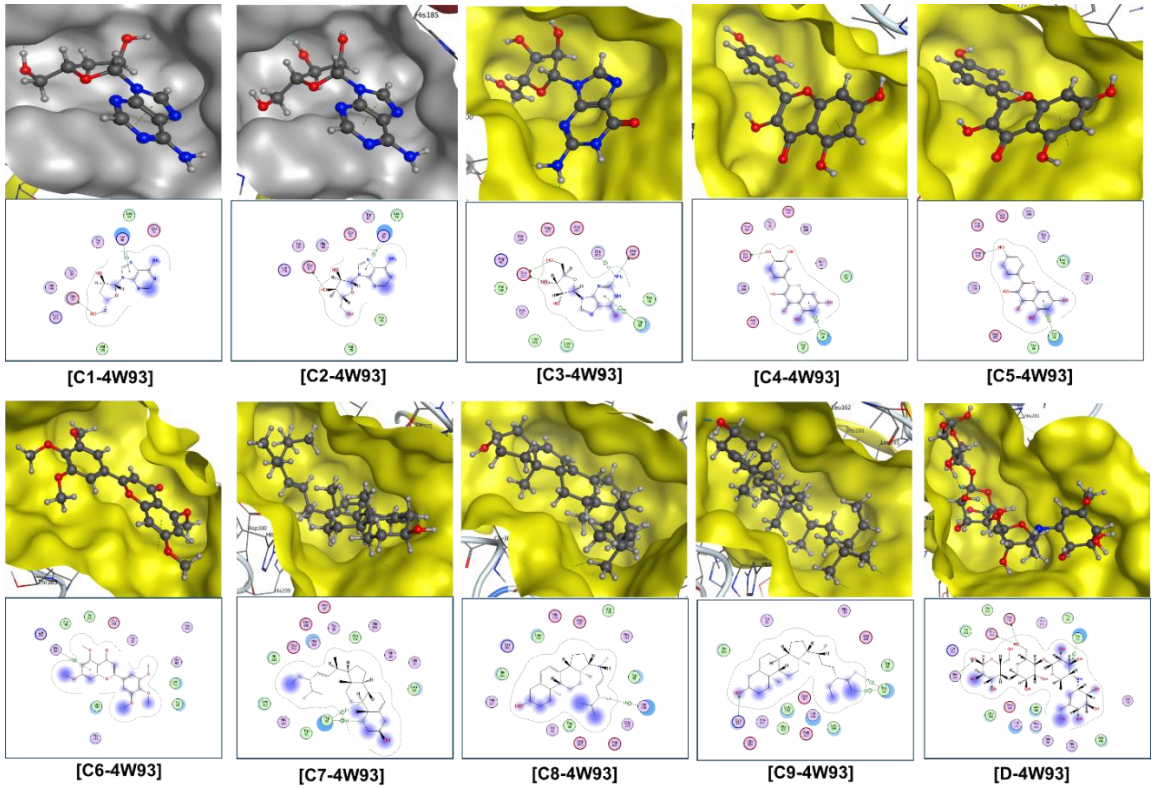

Fig. 4. Visual presentation and in-pose interaction map of ligands (**C1–C9** and **D**)-4W93 inhibitory structures

Table 4. Molecular docking simulation results for ligands (**C1–C9** and **D**)-3W37 inhibitory complexes

Ligand-protein			Hydrogen bond						Van der Waals interaction
Name	DS	RMSD	L		P	T	D	E	
C1-3W37	-11.6	1.09	O	O	Glu 792	H-donor	2.74	-1.3	Gly 791, Thr 790, Asn 758, Tyr 659, Gly 698, Gly 700, Leu 663, Thr 662, Leu 669, Leu 793, Ile 759
			N	O	Asp 666	H-donor	3.12	-1.8	
			O	N	Arg 699	H-acceptor	3.37	-0.5	
C2-3W37	-12.9	1.95	O	O	Asp 469	H-donor	3.10	-1.3	Arg 552, Asp 232, Asp 568, Trp 467, Ile 396, Ile 358, His 626
			O	O	Asp 357	H-donor	2.90	-2.1	
			C	S	Met 470	H-donor	3.57	-0.9	
			C	5-ring	Trp 329	H-π	3.85	-1.4	
			O	6-ring	Phe 601	H-π	3.34	-0.6	
			5-ring	C	Trp 432	π -H	3.91	-1.2	
C3-3W37	-12.7	0.98	O	S	Met 470	H-donor	3.19	-2.1	Trp 329, Asp 357, Trp 432, Asp 469, Ile 396, Trp 565, Gly 567,
			O	O	Asp 568	H-donor	2.95	-0.8	
			N	O	Asp 232	H-donor	2.90	-1.8	
			N	O	Asp 232	H-donor	3.25	-1.1	
			C	S	Met 470	H-donor	3.69	-1.0	
			C	6-ring	Phe 601	H-π	3.30	-0.5	

pISSN 1859-1388
eISSN 2615-9678

Ligand-protein			Hydrogen bond						Van der Waals interaction
Name	DS	RMSD	L	P		T	D	E	
C4-3W37	-11.9	1.35	O	O	Asp 357	H-donor	2.89	-2.7	Met 470, Phe 601, Asp 469, Trp 467, Asp 232, Arg 552, Trp 432, Trp 565, Asp 568, Ile 396
			O	O	Asp 357	H-donor	3.27	-1.4	
			C	6-ring	Trp 329	H-π	3.84	-0.7	
C5-3W37	-11.3	1.47	O	O	Asp 469	H-donor	3.27	-1.4	Phe 601, Ala 628, Ala 602, Asp 630, Asp 232, Trp 432, Arg 552, Met 470, Asp 568, Ile 396, Ile 358,
			O	O	Asp 357	H-donor	2.65	-1.7	
			C	6-ring	Trp 329	H-π	3.69	-0.5	
C6-3W37	-12.0	1.99	C	5-ring	Trp 329	H-π	3.24	-0.5	Asn 237, Asp 232, Asp 568, Phe 236, Arg 552, Met 470, Phe 601, Ala 628, Asp 357, Asp 469, Trp 432,
			C	6-ring	Trp 329	H-π	3.61	-0.5	
			6-ring	C	Ile 233	π -H	3.36	-0.5	
			6-ring	N	Ala 234	π -H	3.33	-0.5	
C7-3W37	-10.8	1.71	O	N	Lys 506	H-acceptor	3.02	-1.2	Phe 236, Ala 234, Asn 475, Phe 476, Asp 232, Ser 474, Asp 568, Phe 601, Met 470, Arg 552, Trp 565, Asp 469, Asp 357, Trp 432, Ile 396, Ile 358,
			C	6-ring	Trp 329	H-π	3.29	-0.6	
C8-3W37	-11.0	1.04	O	Od1	Asp 630	H-donor	3.09	-1.6	Ala 628, Ala 602, Phe 601, Asp 568, Phe 236, Asp 232, Ile 233, Lys 506, Ser 474, Trp 329, Trp 432, Asn 475,
			O	Od2	Asp 630	H-donor	3.16	-0.8	
			C	6-ring	Phe 476	H-π	3.94	-1.1	
C9-3W37	-8.7	1.55	O	Nz	Lys 506	H-acceptor	2.94	-1.2	Ala 234, Phe 236, Asp 232, Asn 475, Ala 628, Trp 329, Phe 601, Asp 568, Met 470, Phe 476, Ser 474, Trp 467, Arg 552, Trp 432, Asp 357, Ile 396, Ile 358, Asp 469,
D-3W37	-13.0	1.50	O	O	Asp 568	H-donor	3.07	-0.6	Ala 628, Asn 475, Trp 329, Phe 601, Phe 236, Arg 552, Trp 432, Phe 476, Ser 474, Asp 469, Ile 396, His 626, Ile 358, Trp 467, Asp 630
			O	O	Asp 232	H-donor	3.27	-0.5	
			O	O	Asp 357	H-donor	2.70	-4.5	
			O	O	Asp 357	H-donor	2.69	-3.7	
			O	S	Met 470	H-donor	3.13	-1.6	
			C	O	Asp 568	H-donor	3.08	-0.5	
			C	O	Asp 568	H-donor	3.10	-0.6	
			C	S	Met 470	H-donor	3.97	-0.7	
			O	N	Lys 506	H-acceptor	3.15	-2.7	
			O	N	Lys 506	H-acceptor	3,31	-0,5	

DS: Docking score energy (kcal.mol^{-1}); **RMSD**: Root-mean-square deviation (Å); **L**: Ligand; **P**: Protein; **T**: Type; **D**: Distance (Å); **E**: Energy (kcal.mol^{-1})

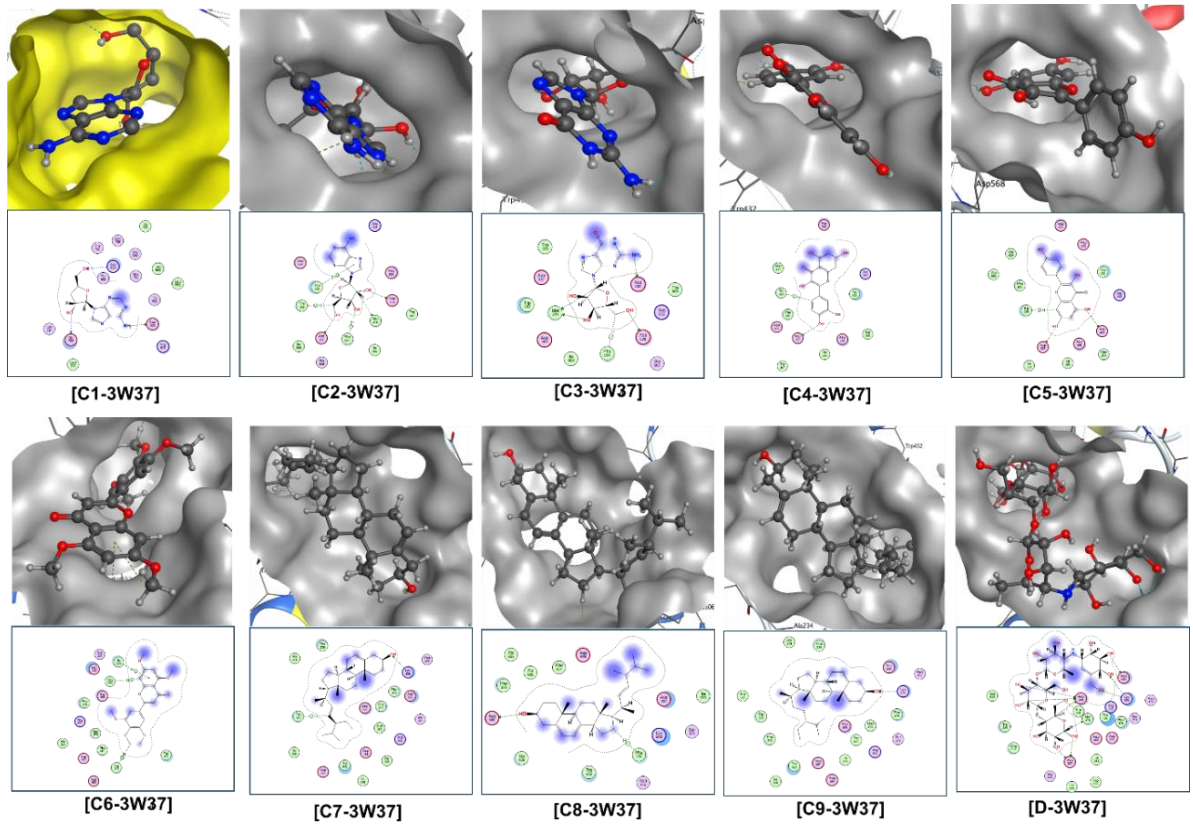

Fig. 5. Visual presentation and in-pose interaction map of ligands (**C1–C9** and **D**)-3W37 inhibitory structures

Table 3 presents the molecular docking results of compounds **C1–C9** and the controlled drug D against protein 4W93, and Fig. 4 shows the 2D-3D simulation images of the inhibition process. According to the docking results, compounds **C1–C9** and the controlled drug **D**, which interact with protein 4W93 through O, N, and C atoms and aromatic rings, formed several key interactions. They include the hydrogen bond (H-donor and H-acceptor) and the π interactions (π-π, H-π) with the amino acids of protein 4W93. Besides, all the RMSD values are below 2 Å, making the results reliable. Among these studied compounds, **C3** showed the strongest inhibitory effect on protein 4W93, which achieved the strongest inhibitory effect on protein 4W93 with a docking score (DS) of –12.4 kcal.mol^{-1}. It exhibited stable binding through three H-donor hydrogen bonds (with Glu233 and Asp356), two π interactions (with His305 and Trp59), and nine van der Waals contacts. The DS values of the studied compounds resulted in the descending order of inhibitory activity against protein 4W93, as follows: **C3-4W93** (–12.4 kcal.mol^{-1}) > **D-4W93** (–12.0 kcal.mol^{-1}) > **C7-4W93** (–11.9 kcal.mol^{-1}) > **C9-4W93** (–11.3 kcal.mol^{-1}) > **C4-4W93** (–11.0 kcal.mol^{-1}) > **C2-4W93** (–10.9 kcal.mol^{-1}) > **C1-4W93** (–10.7 kcal.mol^{-1}) > **C5-4W93** (–10.5 kcal.mol^{-1}) > **C6-4W93** (–9.0 kcal.mol^{-1}) > **C8-4W93** (–8.9 kcal.mol^{-1}). When comparing this result with the controlled drug **D** (DS = –12.0 kcal.mol^{-1}), one can see that compound **C3** shows stronger inhibition towards protein 4W93. Among the studied compounds, **C3, C7**, and **C9** emerge as promising candidates for inhibiting protein 4W93, opening a potential direction for the development of new inhibitors.

The inhibitory activity of compounds **C1–C9** toward protein 3W37 was further evaluated. The results of docking simulations are

pISSN 1859-1388
eISSN 2615-9678

summarised in Table 4. Fig. 5 illustrates the 2D-3D images of binding interactions. In terms of protein 3W37, all RMSD values for the docking process were under 2 Å, confirming the meaningfulness of the docking results. Among the nine studied compounds, **C2** exhibited the strongest inhibitory activity with a docking score of –12.9 kcal.mol^{-1}, involving three H-donor hydrogen bonds, two H-π bonds, and one π-H bond. In contrast, **C9** exhibited the weakest inhibition with a docking score of –8.7 kcal.mol^{-1}, forming only one H-acceptor hydrogen bond. The descending order of inhibitory activity against protein 3W37 is as follows: **D-3W37** (–13.0 kcal.mol^{-1}) > **C2-3W37** (–12.9 kcal.mol^{-1}) > **C3-3W37** (–12.7 kcal.mol^{-1}) > **C6-3W37** (–12.0 kcal.mol^{-1}) > **C4-3W37** (–11.9 kcal.mol^{-1}) > **C1-3W37** (–11.6 kcal.mol^{-1}) > **C5-3W37** (–11.3 kcal.mol^{-1}) > **C8-3W37** (–11.0 kcal.mol^{-1}) > **C7-3W37** (–10.8 kcal.mol^{-1}) > **C9-3W37** (–8.7 kcal.mol^{-1}). Compounds **C2**, **C3,** and **C6** displayed strong inhibitory potential against protein 3W37.

3.3 Physicochemical analysis

The physicochemical parameters of the studied compounds **C1–C9** and the controlled drug, acarbose, namely molecular weight, polarisability, volume, and dispersion coefficients log*P* and log*S*, are presented in Table 5. According to Lipinski's Rule of Five, compounds **C1–C6** satisfy the rules, with the molecular weights ranging from 251.1 to 372.12 Da, the log*P* values from –1.86 to 2.33, and the hydrogen bond numbers within the acceptable limits, which indicate favourable physicochemical properties and suggest good oral absorption. In contrast, compounds **C7, C8,** and **C9,** whose log*P* values exceed the threshold of 5 (6.57, 5.44, and 8.00, respectively), were considered less suitable, as the high lipophilicity could reduce water solubility and limit absorption and distribution in the body. Therefore, **C1–C6** demonstrate the best drug-likeness potential with physicochemical properties that serve as supporting evidence for future drug development research.

Table 5. Physicochemical properties of studied compounds **C1–C9** and Acarbose (**D**)

Compound	Volume	Mass	Polarizability	Dispersion coefficients		Hydrogen-bond count 4W93/3W37
				LogS	LogP	
C1	226.66	251.10	24.14	-1.62	-0.44	2/3
C2	235.45	267.10	24.82	-1.68	-1.13	2/6
C3	244.24	283.09	25.39	-2.18	-1.86	5/6
C4	282.77	302.04	29.15	-3.72	1.45	2/3
C5	273.98	286.05	28.49	-3.65	1.97	2/3
C6	369.25	372.12	38.94	-4.01	2.33	1/4
C7	479.43	412.37	51.38	-5.73	6.57	3/2
C8	459.50	396.34	49.33	-5.13	5.44	1/3
C9	482.07	414.39	51.59	-7.22	8.00	3/1
D	573.32	645.25	56.88	0.53	-4.81	4/10

3.4 ADMET prediction

Table 6. ADMET-based pharmacokinetics and pharmacology of the studied compounds **C1–C5**

Properties	C1	C2	C3	C4	C5	Unit
Absorption						
Water solubility	-2,325	-2,346	-2,544	-2,925	-3,04	(1)
Caco2 permeability	0,119	-0,596	0,061	-0,229	0,032	(2)
Intestinal absorption (human)	70,846	61,243	44,761	77,207	74,29	(3)
Skin Permeability	-2,735	-2,735	-2,735	-2,735	-2,735	(4)
P-glycoprotein substrate	Yes	No	No	Yes	Yes	(5)
P-glycoprotein I inhibitor	No	No	No	No	No	(5)
P-glycoprotein II inhibitor	No	No	No	No	No	(5)
Distribution						
VDss (human)	0,102	0,844	0,316	1,559	1,274	(6)
Fraction unbound (human)	0,699	0,721	0,915	0,206	0,178	(6)
BBB permeability	-1,138	-1,23	-1,272	-1,098	-0,939	(7)
CNS permeability	-3,387	-3,701	-3,944	-3,065	-2,228	(8)
Metabolism						
CYP2D6 substrate	No	No	No	No	No	(5)
CYP3A4 substrate	No	No	No	No	No	(5)
CYP1A2 inhibitor	No	No	No	Yes	Yes	(5)
CYP2C19 inhibitor	No	No	No	No	No	(5)
CYP2C9 inhibitor	No	No	No	No	No	(5)
CYP2D6 inhibitor	No	No	No	No	No	(5)
CYP3A4 inhibitor	No	No	No	No	No	(5)
Excretion						
Total Clearance	0,887	0,763	0,735	0,407	0,477	(9)
Renal OCT2 substrate	No	No	No	No	No	(5)
Toxicity						
AMES toxicity	No	No	No	No	No	(5)
Max. tolerated dose (human)	0,959	0,848	0,198	0,499	0,531	(10)
hERG I inhibitor	No	No	No	No	No	(5)
hERG II inhibitor	No	No	No	No	No	(5)
Oral Rat Acute Toxicity (LD50)	1,685	1,864	2,375	2,471	2,449	(11)
Oral Rat Chronic Toxicity (LOAEL)	2,518	3,366	3,006	2,612	2,505	(12)
Hepatotoxicity	Yes	No	Yes	No	No	(5)

pISSN 1859-1388
eISSN 2615-9678

Properties	C1	C2	C3	C4	C5	Unit
Skin Sensitisation	No	No	No	No	No	(5)
T. pyriformis toxicity	0,285	0,285	0,285	0,288	0,312	(13)
Minnow toxicity	3,236	3,612	4,994	3,721	2,885	(14)

(1) log mol.L^{-1}; (2) log Papp (10^{-6} cm.s^{-1}); (3) %; (4) log Kp; (5) Yes/No; (6) log L.kg^{-1}; (7) log BB; (8) log PS; (9) log mL.min^{-1}.kg^{-1}; (10) log mg.kg^{-1}.day^{-1}; (11) mol.kg^{-1}; (12) log mg.kg^{-1}_bw.day^{-1}; (13) log μg.L^{-1}; (14) log mM

Table 7. ADMET-based pharmacokinetics and pharmacology of the studied compounds **C6–C9** and **D**

Properties	C6	C7	C8	C9	D	Unit
Absorption						
Water solubility	-4,643	-6,682	-6,696	-6,773	-1,482	(1)
Caco2 permeability	1,222	1,213	1,218	1,201	-0,481	(2)
Intestinal absorption (human)	97,42	94,97	95,41	94,464	4,172	(3)
Skin Permeability	-2,684	-2,783	-2,811	-2,783	-2,735	(4)
P-glycoprotein substrate	No	No	No	No	Yes	(5)
P-glycoprotein I inhibitor	Yes	Yes	Yes	Yes	No	(5)
P-glycoprotein II inhibitor	Yes	Yes	Yes	Yes	No	(5)
Distribution						
VDss (human)	-0,195	0,178	0,272	0,193	-0,836	(6)
Fraction unbound (human)	0,104	0	0	0	0,505	(6)
BBB permeability	-0,997	0,771	0,764	0,781	-1,717	(7)
CNS permeability	-3,21	-1,652	-1,752	-1,705	-6,438	(8)
Metabolism						
CYP2D6 substrate	No	No	No	No	No	(5)
CYP3A4 substrate	Yes	Yes	Yes	Yes	No	(5)
CYP1A2 inhibitor	Yes	No	No	No	No	(5)
CYP2C19 inhibitor	Yes	No	No	No	No	(5)
CYP2C9 inhibitor	Yes	No	No	No	No	(5)
CYP2D6 inhibitor	No	No	No	No	No	(5)
CYP3A4 inhibitor	Yes	No	No	No	No	(5)
Excretion						
Total Clearance	0,819	0,618	0,564	0,628	0,428	(9)
Renal OCT2 substrate	Yes	No	No	No	No	(5)
Toxicity						
AMES toxicity	No	No	No	No	No	(5)
Max. tolerated dose (human)	0,371	-0,664	-0,691	-0,621	0,435	(10)
hERG I inhibitor	No	No	No	No	No	(5)
hERG II inhibitor	No	Yes	Yes	Yes	Yes	(5)
Oral Rat Acute Toxicity (LD50)	2,544	2,54	2,255	2,552	2,449	(11)
Oral Rat Chronic Toxicity (LOAEL)	0,977	0,872	0,883	0,855	5,319	(12)

Properties	C6	C7	C8	C9	D	Unit
Hepatotoxicity	No	No	No	No	No	(5)
Skin Sensitisation	No	No	No	No	No	(5)
T. pyriformis toxicity	0,361	0,433	0,517	0,43	0,285	(13)
Minnow toxicity	0,89	-1,675	-1,637	-1,802	16,823	(14)

(1) log mol.L^{-1}; (2) log Papp (10^{-6} cm.s^{-1}); (3) %; (4) log Kp; (5) Yes/No; (6) log L.kg^{-1}; (7) log BB; (8) log PS; (9) log mL.min^{-1}.kg^{-1}; (10) log mg.kg^{-1}.day^{-1}; (11) mol.kg^{-1}; (12) log mg.kg^{-1}_bw.day^{-1}; (13) log μg.L^{-1}; (14) log mM

The pharmacokinetic and toxicological properties of compounds **C1–C9** and the controlled drug **D** were evaluated by using the regression model of SwissADME. The analysis focused on absorption, distribution, metabolism, excretion, and toxicity, which are key parameters in drug development for early screening and selection of safe and effective candidates before *in vitro* and clinical trials.

The investigated compounds are different in terms of absorption. Compounds **C1–C5** had medium to low water solubility (a log*S* from –2.325 to –3.04) and low permeability across the Caco-2 membrane. Besides, compounds **C1**, **C4**, and **C5** were also identified as P-glycoprotein substrates, which could reduce their bioavailability. Compounds **C6–C9**, although having very low solubility (log*S* from –4.643 to –6.773), showed elevated Caco-2 permeability (>1.2), leading to a predicted intestinal absorption rate above 94%, and thus were considered suitable for oral absorption.

Regarding distribution, compounds **C4** and **C5** had high VDss values of 1.559 and 1.274, respectively, indicating their ability to distribute deeply into tissues. Compounds **C7**, **C8**, and **C9** had a fraction unbound in plasma equal to zero, indicating an augmented level of plasma protein binding that could limit their activity. All compounds were predicted to have poor blood-brain barrier (BBB) permeability; therefore, their diffusion and transport into the brain were restricted.

In terms of metabolism and excretion, most compounds from **C1–C9** showed no significant interaction with either Cytochrome P450 enzymes or OCT2, thereby being less metabolised by the liver and failed to inhibit excretion, leading to longer activity in the body. Most compounds were predicted to be efficiently eliminated and thus might not rely on OCT2-mediated renal transport, contributing to favourable pharmacokinetics. The absence of OCT2 inhibition also suggested a low risk of drug-drug interactions and stable clearance.

Regarding toxicity, all compounds gave negative results in the AMES toxicity test, indicating no mutagenic potential. However, other significant risks were identified. Compounds **C7**, **C8**, and **C9** acted as hERG II channel inhibitors, which is a serious warning for potential cardiotoxicity. For hepatotoxicity, **C1** and **C3** were predicted to cause liver damage. All compounds showed low Oral Rat Acute Toxicity and were not associated with skin sensitisation.

3.5 Molecular dynamics simulation

The molecular docking simulations of compounds **C1–C9** against proteins 4W93 and 3W37 were first conducted. The results revealed that **C3** is the most potent inhibitor toward 4W93, and **C2** is the strongest inhibitor toward 3W37; both were chosen for the detailed evaluation of binding interactions through 100 ns molecular dynamics simulations. The protein-ligand complexes were labeled as **[C3–4W93]** in blue and **[C2–3W37]** in pink.

pISSN 1859-1388
eISSN 2615-9678

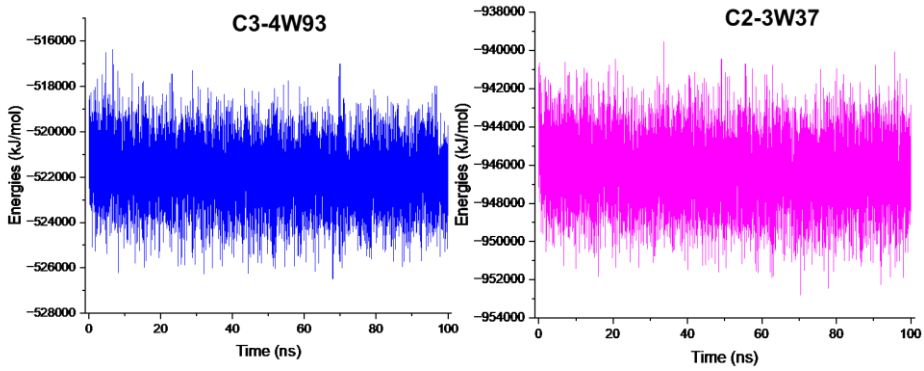

Fig. 6. The energy system of [**C3-4W93**] and [**C2-3W37**]

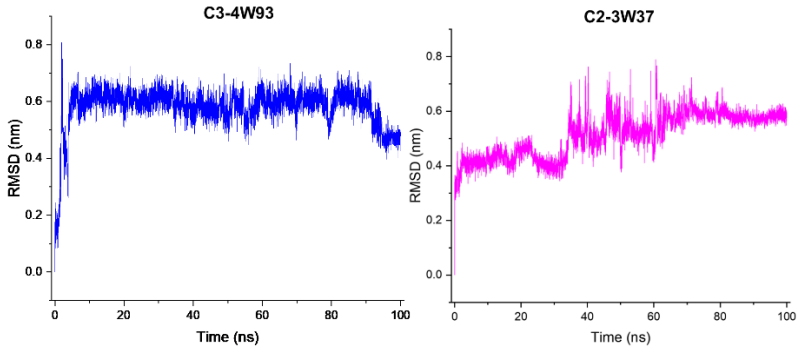

Fig. 7. The RMSD values of [C3-4W93] and [C2-3W37]

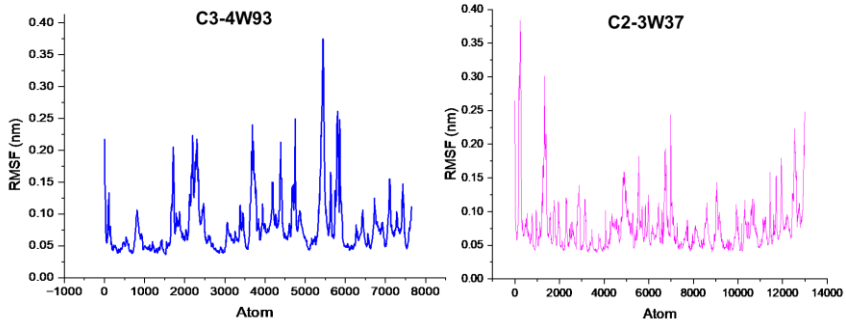

Fig. 8. The RMSF values of [C3-4W93] and [C2-3W37]

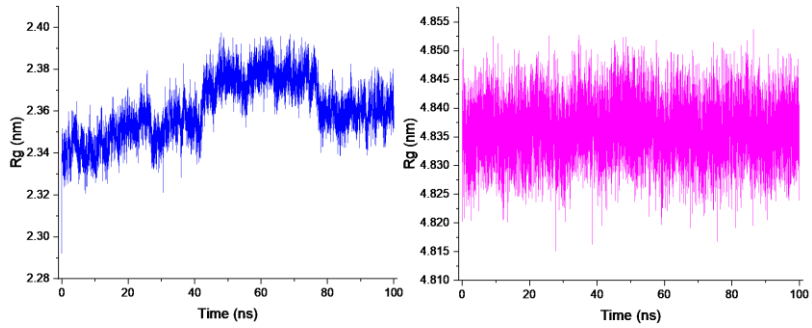

Fig. 9. The Rg values of [C3-4W93] and [C2-3W37]

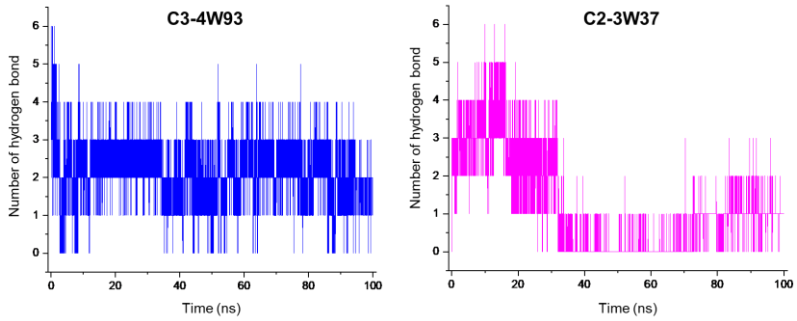

Fig. 10. Number of hydrogen bond of [C3-4W93] and [C2-3W37]

The energies of the **C3-4W93** and **C2-3W37** complexes were analysed, and the results are illustrated in Fig. 6. Both complexes exhibit their energies fluctuating around a stable mean value, confirming that the systems achieved a steady state and could bind stably to the two proteins. Besides, the RMSD values were calculated (Fig. 7), and the results show that the **C3-4W93** system is more stable than the **C2-3W37** system because the latter underwent a large conformational transition at 30–50 ns, which pushed the RMSD up (~0.6 nm), indicating that compound **C3** tends to maintain a more stable protein structure than **C2**. Fig. 8 illustrates the RMSF values of the amino acid residues in the proteins after 100 ns of molecular dynamics simulation, representing the average fluctuation of each residue along the trajectory. In general, both **C3-4W93** and **C2-3W37** complexes exhibited relatively stable fluctuations throughout the simulation. When combined with the radius of gyration data of the amino acids (Fig. 9), which showed only minor variations within 100 ns, these findings suggest that the overall structures of proteins 4W93 and 3W37 remained stable without notable distortion or compaction upon interaction with ligands **C3** and **C2**.

Fig. 10 presents the changes in the number of hydrogen bonds of the **C3-4W93** and **C2-3W37** complexes during 100 ns simulation. In the case of **C3-4W93**, the system retained about 1–4 hydrogen bonds in a stable manner through the whole simulation, and this stability supports the stronger binding of compound **C3** to protein 4W93. By contrast, the **C2-3W37** complex had about 2–5 hydrogen bonds at the beginning, but after around 30 ns, the number decreased rapidly and remained at 1–2 bonds, matching with the structural change presented in the RMSD plot (Fig. 7). The comparison of molecular dynamics analysis between the two complexes **C3-4W93** and **C2-3W37** revealed that compound **C3** has a tendency to bind tightly to protein 4W93 and has a potential in developing inhibitors toward α-amylase.

4 Conclusion

In this study, nine representative compounds from the *Cordyceps* genus were evaluated for their inhibition toward protein 4W93 (*α*-amylase) and protein 3W37 (*α*-glucosidase) with the *in silico* method. The binding sites of 4W93 and 3W37 were screened, and an optimal site was identified. All compounds had root-mean-square deviation (RMSD) values for ligand-protein below 2 Å, indicating reliable docking. The comparison of docking energies resulted in a descending order of inhibitory potential toward the two proteins, as follows: **C3-4W93 > D-4W93 > C7-4W93 > C9-4W93 > C4-4W93 > C2-4W93 > C1-4W93 > C5-4W93 > C6-4W93 > C8-4W9**3 for protein 4W93, and **D-3W37 > C2-3W37 > C3-3W37 > C6-3W37 > C4-3W37 > C1-3W37 > C5-3W37 > C8- > C7-3W37**

pISSN 1859-1388
eISSN 2615-9678

> **C9-3W37** for protein 3W37. A drug-likeness profile based on Lipinski's Rule of Five indicated that compounds **C1–C9** have biocompatible features and are suitable for future drug development. Simultaneously, the pharmacokinetic and toxicological properties of **C1–C3** were assessed by using ADMET parameters. The MD simulations showed that all complexes are structurally stable. Among them, ligand **C3** interacts best with protein 4W93.

Acknowledgement

Nguyen Dai Chau was funded by the Master's and PhD. Scholarship Programme of Vingroup Innovation Foundation (VINIF), codes VINIF.2023.ThS.019 and VINIF.2024.ThS.24. This work was also supported by Hue University under the Core Research Program NCTB.DHH.2024.04, and the L'Oreal-UNESCO For Women in Science International Award 2023.

References

1. Sun H, Saeedi P, Karuranga S, Pinkepank M, Ogurtsova K, Duncan BB, et al. IDF diabetes atlas: Global, regional and country-level diabetes prevalence estimates for 2021 and projections for 2045. Diabetes Res Clin Pract. 2022;183:109119.
2. Nagai M, Matsumoto S, Tanuma J, Nguyen DHT, Nguyen DT, Mizushima D, et al. Prevalence of and factors associated with diabetes mellitus among people living with HIV in Vietnam. Glob Heal Med. 2023;5(1):15-22.
3. Hill-Briggs F, Adler NE, Berkowitz SA, Chin MH, Gary-Webb TL, Navas-Acien A, et al. Social determinants of health and diabetes: a scientific review. Diabetes Care. 2021;44(1):258-79.
4. Henning RJ. Type-2 diabetes mellitus and cardiovascular disease. Future Cardiol. 2018;14(6):491-509.
5. Wu Y, Ding Y, Tanaka Y, Zhang W. Risk factors contributing to type 2 diabetes and recent advances in the treatment and prevention. Vol. 11, International journal of medical sciences. Ivyspring International Publisher; 2014. p. 1185-200.
6. Nxumalo W, Elateeq AA, Sun Y. Can *Cordyceps cicadae* be used as an alternative to *Cordyceps militaris* and *Cordyceps sinensis*?–a review. J Ethnopharmacol. 2020;257:112879.
7. Tsai YS, Hsu JH, Lin DPC, Chang HH, Chang WJ, Chen YL, et al. Safety assessment of HEA-enriched *Cordyceps cicadae* Mycelium: A randomized clinical trial. J Am Coll Nutr. 2021;40(2):127-32.
8. Ding Y, Fang Y, Moreno J, Ramanujam J, Jarrell M, Brylinski M. Assessing the similarity of ligand binding conformations with the Contact Mode Score. Comput Biol Chem. 2016;64(1):403-13.
9. Lipinski CA, Lombardo F, Dominy BW, Feeney PJ. Experimental and computational approaches to estimate solubility and permeability in drug discovery and development settings. Adv Drug Deliv Rev. 1997;23:3-25.
10. Mazumdera J, Chakraborty R, Sena S, Vadrab S, Dec B, Ravi TK. Synthesis and biological evaluation of some novel quinoxalinyl triazole derivatives. Der Pharma Chem. 2009;1(2):188-98.
11. Ahsan MJ, Samy JG, Khalilullah H, Nomani MS, Saraswat P, Gaur R, et al. Molecular properties prediction and synthesis of novel 1,3,4-oxadiazole analogues as potent antimicrobial and antitubercular agents. Bioorganic Med Chem Lett. 2011;21(24):7246-50.
12. Pires DEV, Blundell TL, Ascher DB. pkCSM: Predicting small-molecule pharmacokinetic and toxicity properties using graph-based signatures. J Med Chem. 2015;58(9):4066-72.
13. Hess B, Bekker H, Berendsen HJC, Fraaije JGEM. LINCS: A linear constraint solver for molecular simulations. J Comput Chem. 1997;18(12):1463-72.
14. Valdés-Tresanco MS, Valdés-Tresanco ME, Valiente PA, Moreno E. gmx_MMPBSA: a new tool to perform end-state free energy calculations with GROMACS. J Chem Theory Comput. 2021;17(10):6281-91.
15. Phan TV, Nguyen VTV, Nguyen CHH, Vu TT, Tran TD, Le MT, et al. Discovery of AcrAB-TolC pump inhibitors: Virtual screening and molecular dynamics simulation approach. J Biomol Struct Dyn. 2023;41(22):12503-20.
16. Tuli HS, Sharma AK, Sandhu SS, Kashyap D. Cordycepin: a bioactive metabolite with therapeutic potential. Life Sci. 2013;93(23):863-9.
17. Yang FQ, Li SP. Effects of sample preparation methods on the quantification of nucleosides in

natural and cultured Cordyceps. J Pharm Biomed Anal. 2008;48(1):231-5.

18. Das G, Shin HS, Leyva-Gómez G, Prado-Audelo ML Del, Cortes H, Singh YD, et al. *Cordyceps* spp.: A review on its immune-stimulatory and other biological potentials. Front Pharmacol. 2021;11:2250.
19. Yue K, Ye M, Zhou Z, Sun W, Lin X. The genus *Cordyceps*: a chemical and pharmacological review. J Pharm Pharmacol. 2013;65(4):474-93.
20. Chen PX, Wang S, Nie S, Marcone M. Properties of *Cordyceps sinensis*: a review. J Funct Foods. 2013;5(2):550-69.